Am J Transl Res 2025;17(11):8869-8882
www.ajtr.org /ISSN:1943-8141/AJTR0166992

Original Article

Silymarin attenuates cardiac injury and inflammation in adjuvant-induced rheumatoid arthritis rats through activation of the Nrf2/SLC7A11/GPX4 signaling pathway

Jia Chen[1], Zhijing Miao[1], Jingshu Guan[1], Xuzhou Duan[2]

[1]*Department of Cardiology, Shanghai Baoshan Hospital of Integrated Traditional Chinese and Western Medicine, 181 Friendship Road, Baoshan District, Shanghai 201901, China;* [2]*Department of Orthopedics, The First Affiliated Hospital of Naval Medical University, 168 Changhai Road, Yangpu District, Shanghai 200433, China*

Received June 22, 2025; Accepted October 25, 2025; Epub November 15, 2025; Published November 30, 2025

Abstract: Objective: To investigate the protective effects of silymarin (SIL) against adjuvant-induced cardiac injury and inflammation in rats with rheumatoid arthritis (RA) and to elucidate the underlying mechanisms through *in vivo* and *in vitro* experiments. Methods: RA was induced in rats using Freund's complete adjuvant (FCA), which also causes cardiac injury as an extra-articular manifestation of RA. Rats were treated with different doses of SIL to evaluate its cardioprotective effects. Myocardial injury and inflammatory responses were assessed *in vivo*, while cardiac cells with Nuclear factor erythroid-2-related factor 2 (Nrf2) silencing by small interfering RNA (siRNA) were used *in vitro* to clarify the role of the Nrf2/solute carrier family 7 member 11/Glutathione peroxidase 4 (Nrf2/SLC7A11/GPX4) pathway. Inflammatory cytokine levels were measured using enzyme-linked immunosorbent assay (ELISA); myocardial cell viability and proliferation were evaluated by Cell Counting Kit-8 (CCK-8), clonogenic, and 5-Ethynyl-2'-deoxyuridine (EdU) assays; apoptosis was analyzed by flow cytometry; and the expression of Nrf2, SLC7A11, GPX4, and apoptosis-related proteins was determined by real-time quantitative polymerase chain reaction (RT-qPCR) and western blotting (WB). Histopathologic changes were examined by hematoxylin and eosin (H&E) staining. Results: SIL treatment effectively alleviated myocardial cell injury in SiNrf2-induced cardiac cells and significantly reduced the secretion of inflammatory factors interleukin-1 beta (IL-1β), IL-6, IL-17, and tumor necrosis factor-alpha (TNF-α). Furthermore, SIL activated the Nrf2/SLC7A11/GPX4 signaling pathway, improved myocardial tissue morphology, and suppressed apoptosis in RA rats. Conclusion: SIL exerts protective effects against RA-associated cardiac injury and inflammation, primarily through activation of the Nrf2/SLC7A11/GPX4 signaling pathway. These findings provide mechanistic insight and experimental evidence supporting the use of SIL as a therapeutic agent for preventing cardiac complications in RA.

Keywords: Silymarin, rheumatoid arthritis, Nrf2, GPX4, cardiac injury

Introduction

Rheumatoid arthritis (RA) is an autoimmune disorder in which the immune system targets the body's own joints, leading to chronic, progressive arthritis, characterized by joint swelling, pain, and restricted mobility [1-3]. Elevated levels of inflammatory cytokines and mediators contribute to early-onset heart disease in RA patients, leading to increased myocardial injury and cardiac dysfunction [4]. Cardiovascular disease (CVD) represents a major contributor to death among RA patients, with cardiovascular mortality and morbidity rates approximately 50% and 60% higher, respectively, compared to the general population [5]. Systemic inflammation and cardiovascular inflammation in RA promote atherosclerosis and plaque formation, heightening the risk of cardiovascular events such as myocardial infarction and heart failure [6, 7]. Moreover, RA patients exhibit a greater atherosclerotic plaque burden, more extensive calcification, and higher susceptibility to plaque rupture compared with non-RA individuals [5]. In addition to an elevated risk of developing heart failure, RA patients also face a higher like-

https://doi.org/10.62347/WWAV3590

lihood of mortality shortly after experiencing heart failure [8]. Therefore, it is crucial to closely monitor cardiac injury during RA treatment to ensure comprehensive patient care.

Silymarin (SIL) is a natural flavonoid-lignan compound with potent antioxidant, anti-inflammatory, and pro-apoptotic properties [9, 10]. Research has shown that SIL and its main component, silybin, can downregulate tumor necrosis factor-alpha (TNF-α), and inflammatory factors such as interleukin-1 beta (IL-1β), IL-6, and chemokines including CCL4 and CXCL10 in inflammatory rat models [11]. Other studies have demonstrated that SIL exhibits therapeutic efficacy in RA and osteoarthritis [12]. Additionally, SIL exerts cardioprotective effects. For example, Gabrielová et al. reported that 2,3-dehydrosilybin (DHS), a flavonolignan component of *Silybum marianum*, can alleviate myocardial cell injury following hypoxia/reoxygenation by reducing reactive oxygen species (ROS) production [13]. Similarly, Rao et al. showed that SIL protects against myocardial cell death in rats with myocardial infarction by preserving endogenous antioxidant enzymes [14]. Cardiac injury is mediated by multiple mechanisms, among which ferroptosis has emerged as a key contributor [15]. The nuclear factor erythroid-2-related factor 2/solute carrier family 7 member 11/glutathione peroxidase 4 (Nrf2/SLC7A11/GPX4) signaling pathway plays a crucial role in regulating ferroptosis and maintaining cardiac homeostasis [16, 17]. Moreover, Nrf2 plays a crucial role in cellular resistance to oxidative stress and electrophilic stress, representing a promising pharmacologic target for the treatment of chronic diseases such as RA. Silymarin has been shown to protect renal and hepatic tissues by promoting the nuclear translocation of Nrf2 [18]. Conversely, disruption of Nrf2 nuclear localization suppresses Slc7a11 and Gpx4 expression, thereby triggering cardiac ferroptosis. These findings suggest that silymarin may exert similar protective regulatory effects in cardiomyocytes [19]. We hypothesize that SIL enhances the nuclear translocation of Nrf2, thereby upregulating the expression of Slc7a11 and Gpx4, inhibiting ferroptosis and improving cardiac injury and inflammation in RA.

This study aimed to explore the biological functions and molecular mechanisms of SIL in RA-induced myocardial injury and inflammation, providing new insight into its therapeutic value for RA-associated cardiac complications.

Materials and methods

Laboratory animals

The experimental protocol was approved by the Medical Research Ethics Committee of Shanghai University of Traditional Chinese Medicine, and all animal procedures were carried out in accordance with relevant institutional and national guidelines. Sprague-Dawley (SD) rats (250 g-350 g) were obtained from the Experimental Animal Center of Shanghai University of Traditional Chinese Medicine. Animals were housed under controlled environmental conditions (20°C-25°C and 40%-50% humidity), with a standard 12-h light/dark cycle and *ad libitum* access to food and water.

RA was induced by subcutaneous injection of 0.1 mL of Freund's adjuvant (FCA) into the right hind paw. On day 12 post-injection, an additional 0.05 mL of FCA was administered at the base of the rats' tails to boost immunity. Seven days after model establishment, rats were randomly allocated into five groups (n = 12 per group): Control (healthy rats), FCA (RA model), FCA + L (RA + low-dose SIL, 5 mg/kg), FCA + M (RA + medium-dose SIL, 25 mg/kg), and FCA + H (RA + high-dose SIL, 50 mg/kg/d). SIL was administered daily at the same time for four consecutive weeks. At the end of the study, animals were anesthetized with sodium pentobarbital (150 mg/kg, intraperitoneally) and euthanized by exsanguination, in compliance with the AVMA Guidelines for the Euthanasia of Animals.

Cell treatment

H9C2 cardiomyocytes were obtained from Shanghai GeneChem Co., Ltd. Cells were cultured under standard conditions and stimulated with 1 μg/mL lipopolysaccharide (LPS) for 4 h to induce myocardial injury, thus establishing an *in vitro* model of cardiac damage [20].

Cell transfection

Small interfering RNA targeting Nrf2 (SiNrf2), the Nrf2 inhibitor, and negative control (siNC) were synthesized by Shanghai GeneChem Co., Ltd. The sequence were as follows: Nrf2 siRNA, 5'-GGAUGAAGAGACCGGAGAAUU-3'; neg-

Table 1. Primer sequence for RT-qPCR

Gene	Forward (5'-3')	Reverse (5'-3')
Nrf2	CCCAGCACATCCAGACAGAC	TATCCAGGGCAAGCGACTC
GPX4	CTCCATGCACGAATTCTCAG	ACGTCAGTTTTGCCTCATTG
SLC7A11	TCTCCAAAGGAGGTTACCTGC	AGACTCCCCTCAGTAAAGTGAC
Bax	CTGCAGAGGATGATTGCTG	GTCTGCAAACATGTCAGCT
Bcl2	TGACTGAGTACCTGAACCG	TAGTTCCACAAAGGCATCC
GAPDH	GCGAGATCCCGCTAACATCA	ATTCGAGAGAAGGGAGGGCT

ative control siRNA (siNC), 5'-GAUAAAAGG-GUAAGGUGACCG-3'. Cell transfection was carried out utilizing Lipofectamine 2000 (Invitrogen, USA; Cat. No. 11668) according to the manufacturer's instructions. The efficiency of Nrf2 knockdown was verified through PCR and WB analysis after 48 h.

Enzyme-Linked Immunosorbent Assay (ELISA)

Serum levels of IL-1β (SEKM-0002, Solarbio, China), IL-6 (SEKM-0007, Solarbio, China), TNF-α (CLP0771, Solarbio, China), and IL-17 (SEKM-0017, Solarbio, China) were determined using commercial ELISA kits. Briefly, serum samples were added to antibody-coated wells and incubated according to the kit protocol. After washing to remove unbound substances, enzyme-conjugated detection antibodies were added, followed by substrate solution to produce a colorimetric reaction. The absorbance was measured at 450 nm using a microplate reader.

Ultrasound echocardiography

Rats were weighed, and the appropriate dose of sodium pentobarbital (50 mg/kg) was calculated and administered intraperitoneally to induce anesthesia. Subsequently, each rat was placed in a suitable position, and a pressure-volume sensor was inserted into its left ventricle via the right carotid artery. Upon successful insertion, the sensor was carefully secured to prevent displacement. Hemodynamic values only, including heart rate (HR), left ventricular systolic pressure (LVSP), and left ventricular end-diastolic pressure (LVEDP), were recorded using the MS4000U-1C Biological Signal Quantitative Recording and Analysis System. System parameters were calibrated before data acquisition to ensure measurement accuracy.

Histopathologic examination

Fresh cardiac tissue samples were collected and rinsed in pre-cooled phosphate-buffered saline (PBS), gently dried with clean filter paper, and fixed in 4% paraformaldehyde for over 24 h. Fixed tissues were dehydrated through a gradient ethanol series, cleared with xylene, and embedded in paraffin. Sections of 5 μm thickness were cut using a microtome, mounted on glass slides, and stained with hematoxylin and eosin (H&E). After staining, slides were dehydrated, cleared, sealed with neutral resin, and examined.

Real-time quantitative polymerase chain reaction (RT-qPCR)

Total RNA was extracted from cardiac tissues or cultured cells using TRIzol and then converted to cDNA using the PrimeScript RT kit (RR037A, TAKARA, JAPAN) according to the manufacturer's instructions. RT-qPCR was performed using a PCR instrument. The primer sequences are shown in **Table 1**.

Western blotting (WB)

Total protein was extracted from cardiac tissue and cultured cells, and the concentration was determined using the Bicinchoninic Acid (BCA) protein assay kit (23227, Invitrogen, USA). Equal amounts of protein (30 μg per lane) were separated by sodium dodecyl sulfate-polyacrylamide gel electrophoresis (SDS-PAGE) and transferred onto polyvinylidene fluoride (PVDF) membranes. The membranes were blocked in Tris-buffered saline containing Tween-20 (TBST) supplemented with 5% skim milk for 1 h at room temperature to prevent nonspecific binding.

Subsequently, the membranes were incubated overnight at 4°C with the primary antibodies: anti-SLC7A11 (1:1000, ab175186; Abcam), anti-GPX4 (1:10000, ab125066, Abcam, USA), anti-Nrf2 (1:1000, ab62352, Abcam), and anti-GAPDH (1:1000, ab8245, Abcam, USA). The next day, the membranes were washed with PBS three times to remove unbound antibodies, followed by incubation with the corresponding secondary antibodies (1:1000, ab-150077, Abcam, USA) for 1 h. After washing

again, an enhanced chemiluminescence (ECL) detection reagent was used to visualize the protein bands. The protein bands were quantified using ImageJ software, with GAPDH as an internal reference.

Immunohistochemistry (IHC)

Cardiac tissue sections were deparaffinized, rehydrated, and washed with PBS. After antigen retrieval, sections were blocked with bovine serum albumin (BSA) and incubated overnight at 4°C with primary antibodies against GPX4, Nrf2, and SLC7A11 (Abcam, USA). The next day, sections were washed with PBS and incubated with appropriate secondary antibodies for 20 min at room temperature. Following additional PBS washes, color development was performed using DAB substrate, and nuclei were counterstained with hematoxylin. Stained sections were dehydrated, mounted, and examined to assess protein expression and localization.

Cell viability assay

Cell viability was assessed using the CCK-8 assay kit (BIO-(tw)-1219, Invitrogen, USA). H9C2 cells were uniformly seeded in 6-well plates and treated with various concentrations of SIL (0, 25, 50, 75, 100, and 150 μg/mL). At 0 h, 24 h, 48 h, and 72 h after treatment, 10 μL of CCK-8 solution was added to each well, followed by incubation for 2 h at 37°C. Absorbance was measured at 450 nm using a calibrated microplate reader, and the optical density (OD) values at each time point were recorded to determine cell viability.

Colony formation assay

H9C2 cells were divided into three groups: Control (untreated myocardial cells), LPS group (LPS-induced myocardial injury), and LPS + SIL group (LPS-induced myocardial injury treated with 50 μg/mL SIL). Cells were seeded at a density of 1×10^5 cells/well in DMEM containing 10% FBS and cultured at 37°C in a humidified atmosphere with 5% CO_2 for 15 days until visible colonies formed. After removing the culture medium, cells were fixed with pure methanol for 15 minutes, washed with PBS, and stained with Giemsa solution for 30 minutes. Excess stain was removed by rinsing with distilled water, and plates were air-dried. The number of clones was counted under a microscope.

5-Ethynyl-2'-deoxyuridine (EdU) staining

Cell proliferation was assessed using EdU cell proliferation detection kit (C0088S, Beyotime, China). Cells from the Control, LPS, and LPS + SIL groups were incubated with EdU (20 mmol/L) for 2 h. Subsequently, the cells were fixed with Immunostaining Fixation Solution (P0098) for 20 minutes, permeabilized with Immunostaining Permeabilization Buffer (P0097) for 15 minutes, and then treated with 200 μL of Click reaction mixture for 1 h in the dark with gentle shaking. After washing, 20 μl of Streptavidin-HRP working solution was added and incubated for 30 minutes, followed by 100 μL of TMB chromogenic solution for 15 minutes. The stained EdU-positive nuclei were visualized and quantified using a fluorescence microscope.

Flow cytometry assay

Apoptosis was evaluated using the Annexin V-fluorescein isothiocyanate and propidium iodide (PI) apoptosis detection kit (abx290007, Abbexa, UK). Cells from the Control, LPS, and LPS + SIL groups were cultured for 48 h. Then, 10 μl of PI staining working solution was added and incubated for 15 minutes at room temperature in the dark. Subsequently, 300 μl of binding buffer was added, and cell apoptosis was detected within 1 h using a BD FACSCalibur flow cytometer.

Statistical analysis

All data were analyzed using GraphPad Prism 9.3 statistical software. Data were expressed as mean ± standard deviation (SD). Comparisons between two groups were performed using Student's t-test, while comparisons among multiple groups were analyzed by one-way analysis of variance (ANOVA) followed by Tukey's post hoc test. A p-value < 0.05 was considered statistically significant.

Results

SIL alleviated inflammation in RA rats

Compared to the control group, rats induced with FCA showed significantly increased paw swelling and arthritis scores, confirming the successful establishment of the RA rat model. Compared to the FCA group, SIL treatment sig-

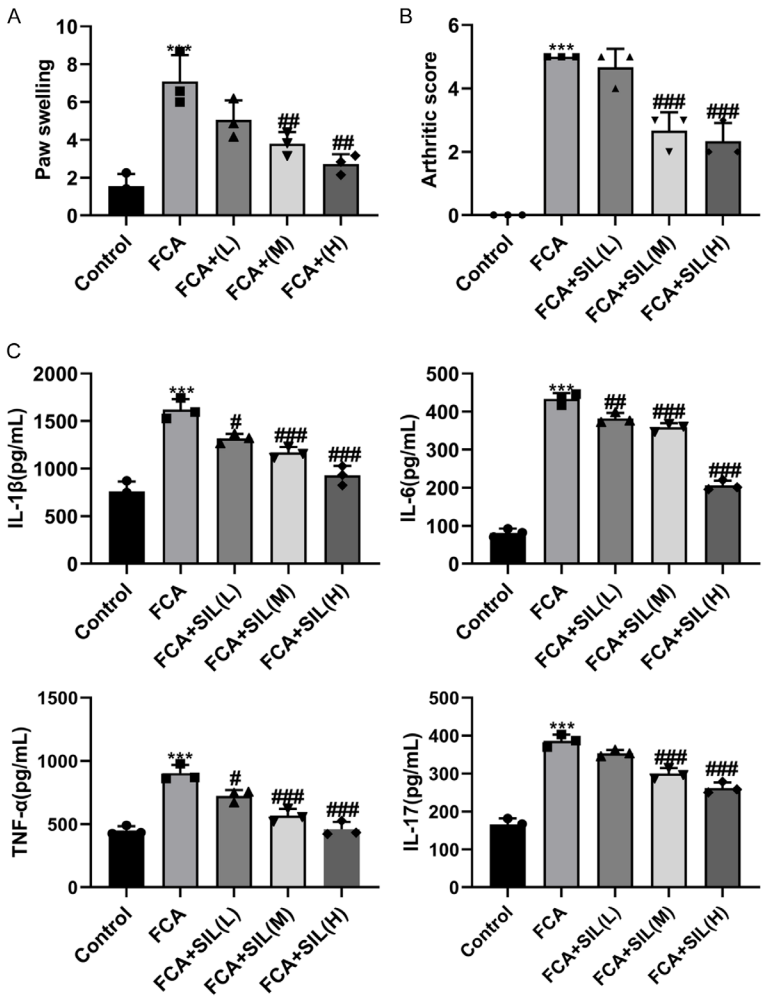

Figure 1. Effects of silymarin (SIL) on inflammation of rheumatoid arthritis (RA) rats. A. Paw swelling in rats from various treatment groups. B. Arthritis scores in rats from various treatment groups. C. Effects of different concentrations of SIL on the serum levels of inflammatory factors in arthritis rats. Data are presented as mean ± SEM (n = 12). $^{***}P < 0.001$, vs. control; $^{\#}P < 0.05$, $^{\#\#}P < 0.01$, $^{\#\#\#}P < 0.001$, vs. FCA.

nificantly reduced paw swelling and arthritis scores in both the FCA + M and FCA + H groups (P < 0.05) (**Figure 1A**, **1B**). Furthermore, serum concentrations of IL-1β, IL-6, TNF-α, and IL-17 were significantly decreased in the FCA + L, FCA + M, and FCA + H groups compared with the FCA group (**Figure 1C**). These results indicate that SIL treatment effectively mitigates systemic inflammation in RA rats.

SIL improved FCA-induced myocardial injury and inflammation in RA rats

To evaluate the cardioprotective effects of SIL, hemodynamic parameters including HR, LVSP, and LVEDP were measured. Rats in the FCA groups exhibited significantly elevated HR, LVSP, and LVEDP compared to the control group (P < 0.05), whereas these values were markedly reduced in the FCA + M and FCA + H groups (P < 0.05) (**Figure 2A**).

Histopathologic analysis further supported these findings. H&E staining revealed disordered myocardial architecture and notable inflammatory cell infiltration in the FCA group. In contrast, these changes were markedly attenuated in the FCA + L, FCA + M, and FCA + H groups, which exhibited more regular cardiomyocyte arrangement and fewer inflammatory cells (**Figure 2B**). Collectively, these results suggest that SIL confers significant protective effects against FCA-induced myocardial alteration and inflammation in RA rats.

SIL alleviated myocardial injury in RA rats via the Nrf2/SLC7A11/GPX4 signaling pathway

Based on our initial hypothesis, we investigated whether the cardioprotective effects of SIL are mediated through the Nrf2/SLC7A11/GPX4 signaling pathway, a key regulator of ferroptosis and cardiac injury. The mRNA and protein levels of Nrf2, SLC7A11, and GPX4 in myocardial tissues of RA rats were assessed by RT-qPCR and western blotting. Compared with the control group, rats in the FCA group exhibited significantly decreased expression of Nrf2, SLC7A11, and GPX4 (P < 0.05). In contrast, these markers were markedly upregulated in the FCA + M and FCA + H groups relative to the FCA group (P < 0.05) (**Figure 3A**, **3B**).

IHC analysis further confirmed these results, showing reduced expression of Nrf2, SLC7A11, and GPX4 in the FCA group, whereas SIL administration restored their expression (**Figure 3C**).

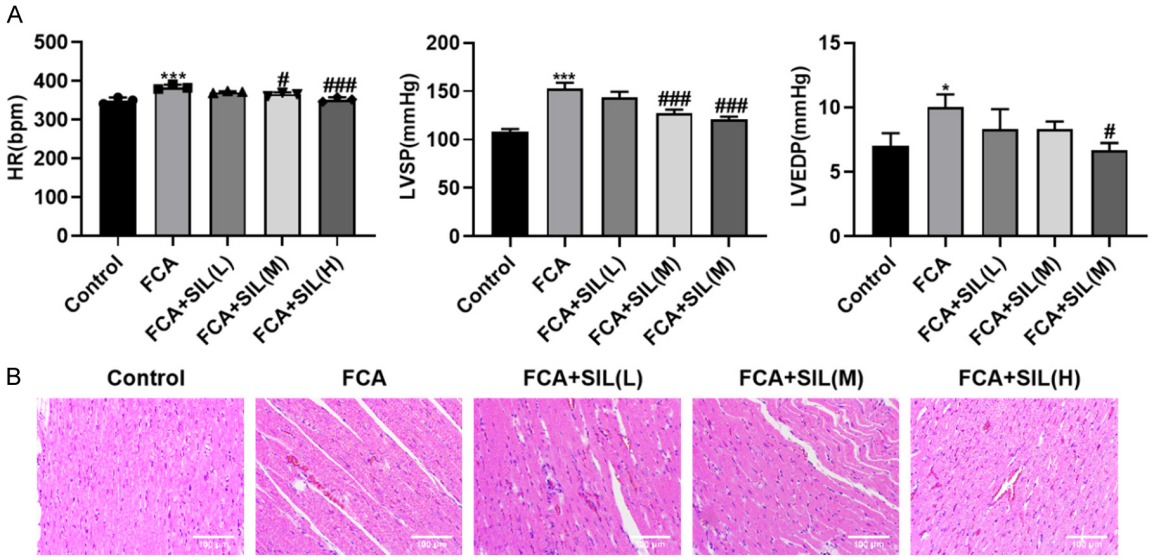

Figure 2. Effects of SIL on cardiac function and myocardial morphology in RA rats. A. Effects of SIL at various concentrations on HR, LVSP, and LVEDP of RA rats. B. Pathologic examination of myocardial tissue in rats from various treatment groups (H&E ×200). Data are presented as mean ± SEM, (n = 12). $^{*}P < 0.05$, $^{***}P < 0.001$, vs. Control; $^{\#}P < 0.05$, $^{\#\#\#}P < 0.001$, vs. FCA.

These results indicate that the cardioprotective effect of SIL in RA rats is at least partly mediated through activation of the Nrf2/SLC7A11/GPX4 signaling pathway.

Toxicity of different concentrations of SIL on H9C2 cells

To evaluate the toxicity of SIL in rat cardiomyocytes, H9C2 cells were treated with different concentrations of SIL (0, 25, 50, 75, 100, and 150 μg/mL). The CCK-8 results showed that compared to the control cells, SIL at of 50 μg/mL exhibited no significant cytotoxicity (**Figure 4A**). Therefore, 50 μg/mL was selected for subsequent experiments to assess its protective effects on myocardial injury. The LPS group displayed a significant increase in LDH content compared with the control group ($P < 0.05$), whereas the LPS + SIL (50 μg/mL) group showed a notable decrease compared to the LPS group ($P < 0.05$) (**Figure 4B**). These findings indicate that SIL at a concentration of 50 μg/mL is non-toxic to H9C2 cells and exerts a protective effect against LPS-induced myocardial injury.

SIL protected H9C2 cells from LPS-induced injury

To elucidate the protective effects of SIL on myocardial injury in RA rats, we assessed cell activity, proliferation, and apoptosis in H9C2 cardiomyocytes treated with 50 μg/mL SIL. The CCK-8 assay revealed a significant increase in cell viability in the LPS + SIL (50 μg/mL) group compared to the LPS group ($P < 0.05$) (**Figure 5A**). Moreover, colony formation and EdU assays demonstrated significantly enhanced cell proliferation in the LPS + SIL group compared to the LPS group ($P < 0.05$) (**Figure 5B**, **5C**).

Flow cytometry analysis demonstrated a significant reduction in apoptosis in the LPS + SIL group in comparison to the LPS group ($P < 0.05$) (**Figure 5D**). WB results further demonstrated a significant decrease in Bax and a notable increase in Bcl2 in the LPS + SIL group, compared to the LPS group ($P < 0.05$) (**Figure 5E**). In addition, SIL treatment significantly decreased the cellular levels of proinflammatory cytokines IL-1β, IL-6, TNF-α, and IL-17 compared to the LPS group rats ($P < 0.05$) (**Figure 5F**). Collectively, these results indicate that SIL has a protective effect on reducing myocardial cell damage and inflammation in RA rats.

SIL activates the Nrf2/SLC7A11/GPX4 signaling pathway

To investigate the mechanism underlying the cardioprotective effects of SIL, Nrf2 expression was silenced in H9C2 cells (**Figure 6A**, **6B**), followed by detection of SLC7A11 and GPX4

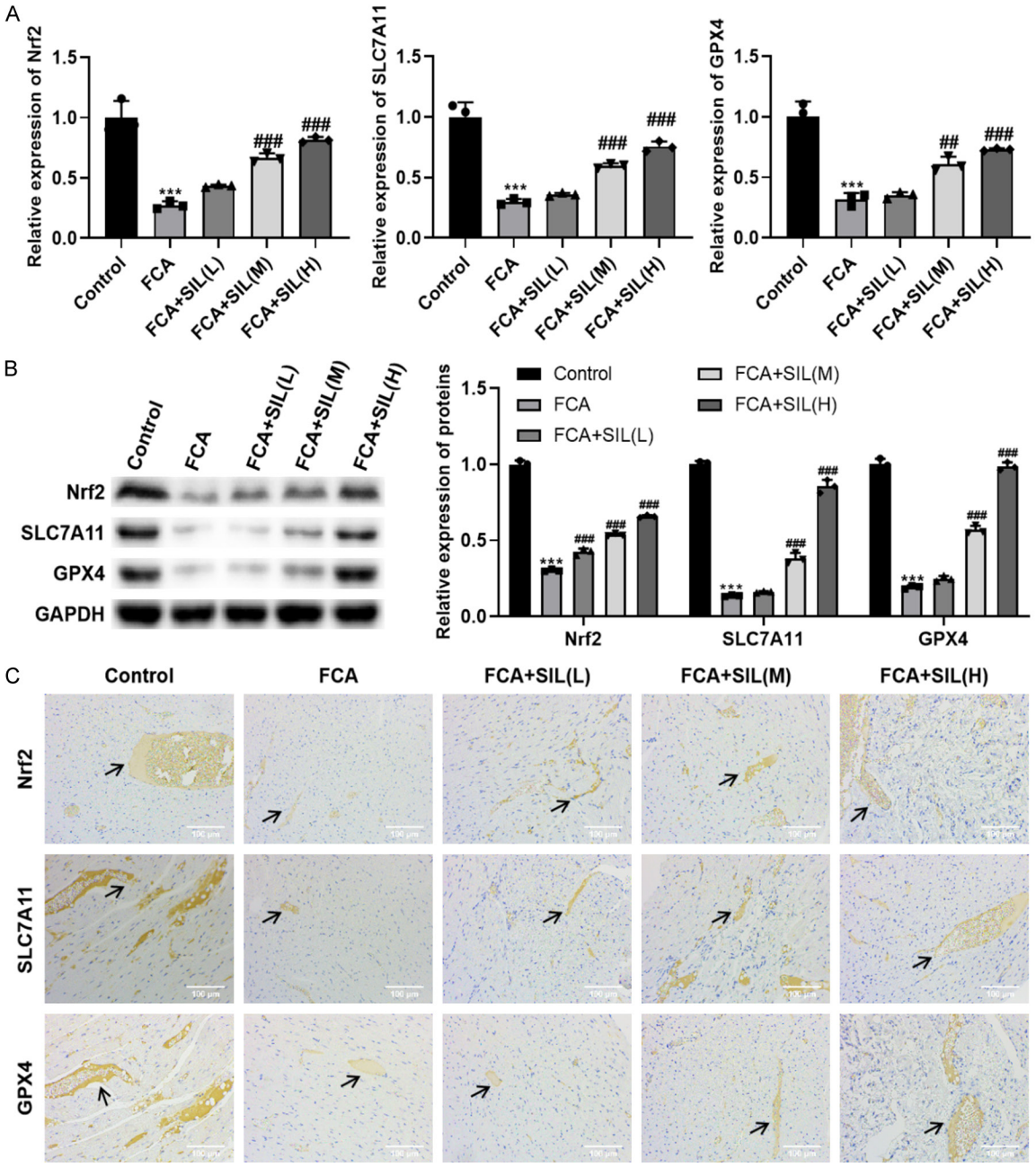

Figure 3. Effects of SIL on the Nrf2/SLC7A11/GPX4 signaling pathway in the cardiac tissue of RA rats. A. mRNA expression levels of Nrf2, SLC7A11, and GPX4. B. Protein expression levels of Nrf2, SLC7A11, and GPX4. C. Immunohistochemistry (IHC) analysis of Nrf2, SLC7A11, and GPX4 contents in myocardial tissues. Positive staining (brownish-yellow) is indicated by black arrows in the images. Nrf2 is predominantly localized in the nucleus, while SLC7A11 and GPX4 are primarily in the cytoplasm. Data are presented as mean ± SEM (n = 12). $^{***}P < 0.001$, vs. control; $^{\#\#}P < 0.01$, $^{\#\#\#}P < 0.001$, vs. FCA.

expression. RT-qPCR results revealed that compared to the LPS group, the mRNA levels of Nrf2, SLC7A11, and GPX4 were significantly upregulated in the LPS + SIL group ($P < 0.05$). However, Nrf2 knockdown markedly reduced the expression of both SLC7A11 and GPX4 (**Figure 6C**). WB results revealed similar results at the protein level (**Figure 6D**). These results confirm that SIL can activate the Nrf2/SLC7A11/GPX4 signaling pathway.

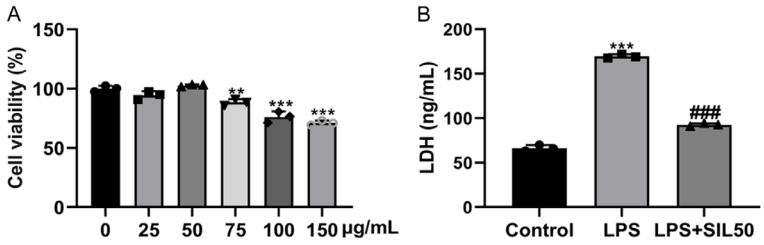

Figure 4. Effects of SIL on cardiomyocyte injury values. A. Cells were treated with 0, 25, 50, 75, 100, and 150 μg/mL of SIL for 24 h, and cell activity was assessed using CCK8. B. The effect of SIL (50 μg/mL) on LDH level in LPS-induced H9C2 cells. Data are presented as mean ± SEM (n = 3). $^{**}P < 0.01$, $^{***}P < 0.001$, vs. control; $^{###}P < 0.001$, vs. LPS.

SIL inhibited LPS-induced myocardial cell injury and inflammation by activating the Nrf2/SLC7A11/GPX4 signaling pathway

The CCK-8 assay revealed a significantly reduced cell viability in the LPS + SIL + siNrf2 group compared to the LPS + SIL + si-NC groups ($P < 0.05$) (**Figure 7A**). Similarly, colony formation and EdU assays demonstrated significant reduction in cell proliferation in the LPS + SIL + siNrf2 group when compared to the LPS + SIL + si-NC groups (**Figure 7B**, **7C**). Flow cytometry analysis further revealed a notable increase in apoptosis in the LPS + SIL + siNrf2 group compared to the LPS + SIL + si-NC group (**Figure 7D**).

WB results showed that compared with the LPS + SIL + si-NC group, Nrf2 knockdown reversed the antiapoptotic effects of SIL, as evidenced by elevated Bax expression and reduced Bcl-2 expression in the LPS + SIL + siNrf2 group ($P < 0.05$) (**Figure 7E**). In addition, ELISA analysis demonstrated significantly increased levels of IL-1β, IL-6, TNF-α, and IL-17 in the LPS + SIL + siNrf2 group compared with the LPS + SIL + si-NC groups ($P < 0.05$) (**Figure 7F**). Collectively, these results demonstrate that SIL protects against LPS-induced myocardial injury and inflammation by activating the Nrf2/SLC7A11/GPX4 signaling pathway.

Discussion

Rheumatoid arthritis (RA) is an autoimmune disease that not only causes joint destruction but also harms cardiac structure and function, increasing the risk of heart failure [21]. The incidence of heart failure in RA patients is two to three times higher than that in the general population [22]. *Silybum marianum*, a medicinal herb of the Asteraceae family, contains SIL as its main component, known for its strong antioxidant, antifibrotic, and anti-inflammatory properties [23]. This study investigated the effects and underlying mechanisms of SIL on myocardial injury and inflammation in RA. Our results demonstrated that SIL markedly reduced the secretion of inflammatory cytokines and enhanced the viability of myocardial cells in RA rats by activating the Nrf2/SLC7A11/GPX4 signaling pathway.

During the pathogenesis of RA, excessive production of inflammatory cytokines plays a key role in disease progression; thus, suppressing cytokine release remains a central therapeutic strategy [24]. Previous studies have shown that SIL significantly alleviates paw swelling in RA rats and reduces cytokine secretion, thereby inhibiting inflammatory responses [25]. Meng et al. discovered that SIL significantly reduced cardiac fibrosis and collagen deposition in diabetic rats, improving cardiac dysfunction [26]. Similarly, Safarpour et al. demonstrated that SIL mitigated 5-Fluorouracil-induced cardiac toxicity and histopathologic degeneration in rats [27]. Consistent with these findings, our results confirmed that SIL significantly alleviated inflammation in both RA rat and cellular models.

SIL may exert its cardioprotective through multiple mechanisms, including modulation of cardiac hemodynamic values, reduction of mechanical dysfunction, and structural remodeling of the myocardium [28]. Additionally, SIL may regulate signaling pathways involved in apoptosis and proliferation, further enhancing its cardioprotective effect [29]. Recent studies have also shown that preoperative administration of SIL significantly decreases the incidence of atrial fibrillation following coronary artery bypass grafting, highlighting its potential in preventing inflammation-associated cardiac arrhythmias [30]. Together, these findings reinforce SIL's potential in reducing RA-induced inflammation and protecting the myocardium.

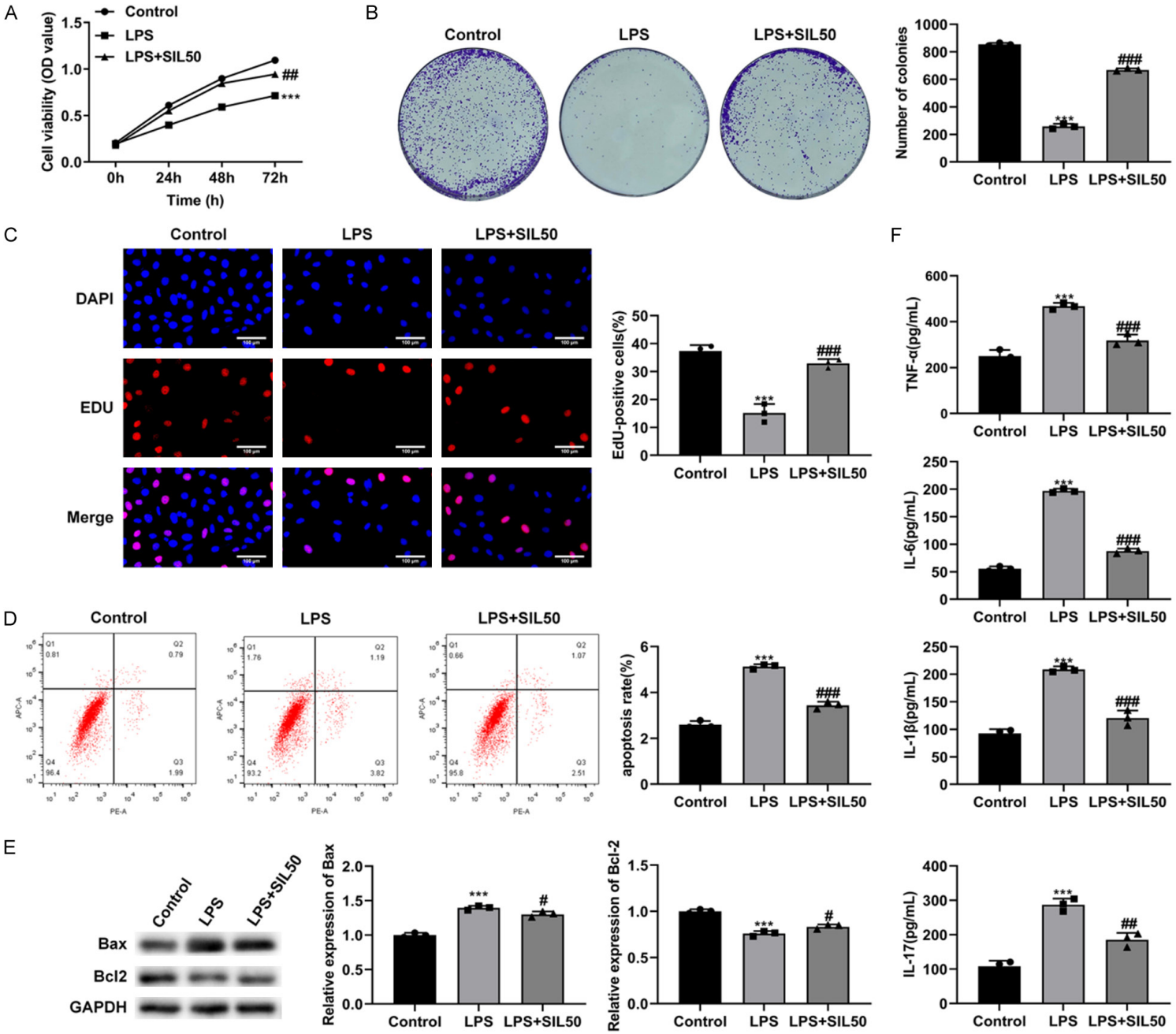
A
Control
LPS
LPS+SIL50
Cell viability (OD value)
Time (h)
0h
24h
48h
72h
##
***
B
Control
LPS
LPS+SIL50
Number of colonies
###
C
DAPI
EDU
Merge
EdU-positive cells(%)
D
apoptosis rate(%)
E
Bax
Bcl2
GAPDH
Relative expression of Bax
Relative expression of Bcl-2
F
TNF-α(pg/mL)
IL-6(pg/mL)
IL-1β(pg/mL)
IL-17(pg/mL)

Figure 5. Effects of SIL on LPS-induced cardiomyocyte injuru. A. Cell activity assessed by Cell Counting Kit-8 (CCK-8) assay. B. Colony formation assay for cell proliferation. C. 5-Ethynyl-2'-deoxyuridine (EdU) staining for cell proliferation. D. Flow cytometry analysis of cell apoptosis. E. WB analysis of apoptosis-related proteins. F. Enzyme-Linked Immunosorbent (ELISA) for inflammatory cytokine levels. Data are presented as mean ± SEM (n = 3). $^{***}P < 0.001$, vs. control; $^{\#}P < 0.05$, $^{\#\#}P < 0.01$, $^{\#\#\#}P < 0.001$, vs. LPS.

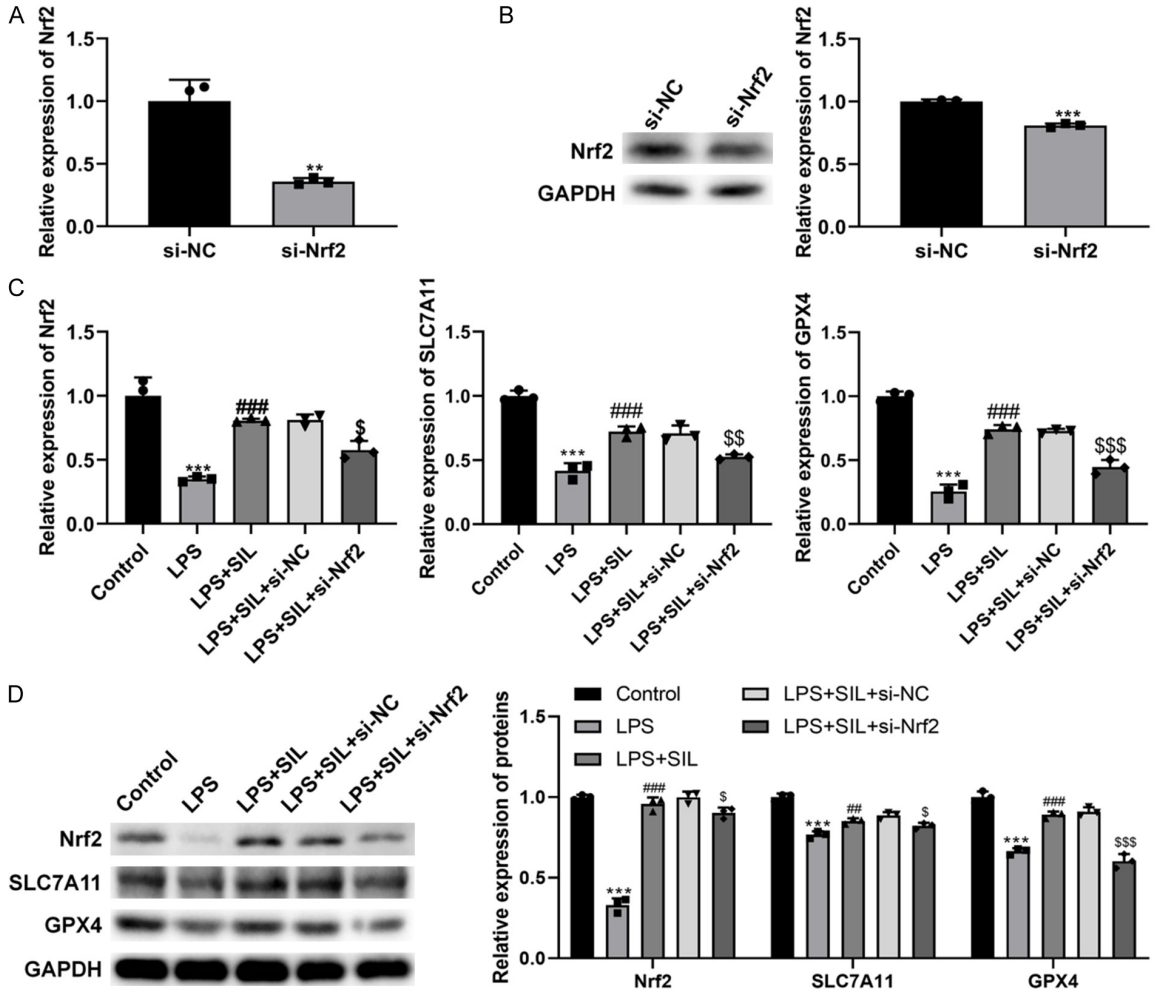

Figure 6. Effects of SIL on the Nrf2/SLC7A11/GPX4 signaling pathway. A. RT-qPCR analysis of Nrf2 knockdown efficiency. B. WB analysis confirming Nrf2 knockdown efficiency. C. RT-qPCR detection of the mRNA expression of Nrf2, SLC7A11, and GPX4. D. WB detection of the protein expression of Nrf2, SLC7A11, and GPX4. Data are presented as mean ± SEM (n = 3). $^{**}P < 0.01$, $^{***}P < 0.001$, vs. si-NC; $^{\#\#}P < 0.01$, $^{\#\#\#}P < 0.001$, vs. LPS; $^{\$}P < 0.05$, $^{\$\$}P < 0.01$, $^{\$\$\$}P < 0.001$, vs. LPS + SIL + si-NC.

To further elucidate the mechanism underlying the therapeutic effects of SIL in RA, we examined its effect on the Nrf2/SLC7A11/GPX4 signaling pathway. Nrf2 is a transcription factor that regulates cellular oxidative stress responses and antioxidant defense mechanisms by controlling the expression of downstream target genes, including SLC7A11 and GPX4 [31]. SLC7A11 is involved in glutathione biosynthesis, regulating cellular oxidative stress responses and resistance to oxidative damage [32]. GPX4, a crucial antioxidant enzyme, eliminates lipid peroxides and protects cell membranes and organelles from oxidative damage [33]. The Nrf2/SLC7A11/GPX4 signaling pathway represents a primary antioxidant defense pathway against ferroptosis [34], which is closely associated with the pathogenesis and progression of human arthritis [35]. Previous studies have provided additional evidence linking this

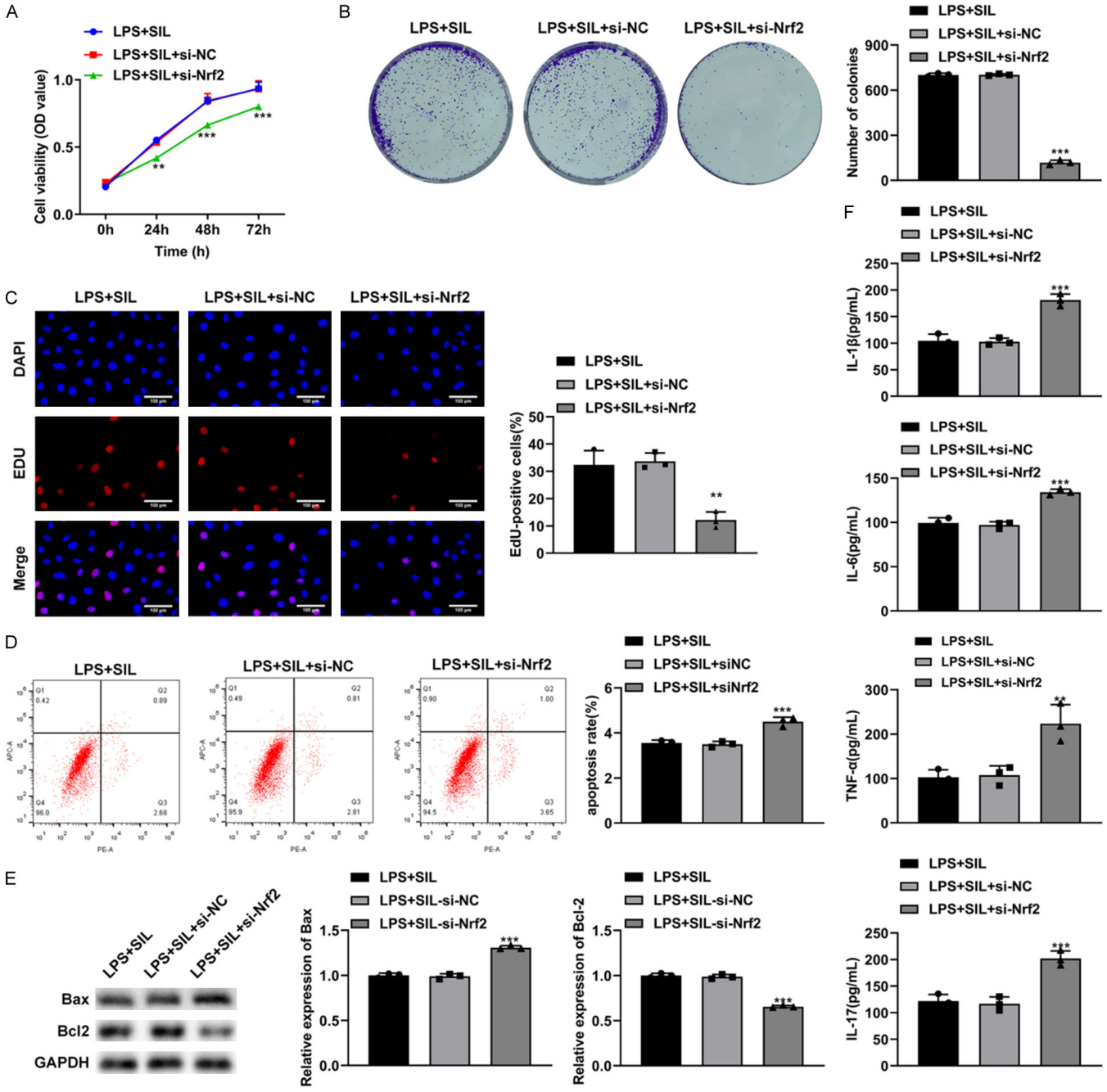
A
LPS+SIL
LPS+SIL+si-NC
LPS+SIL+si-Nrf2
Cell viability (OD value)
Time (h)
0h
24h
48h
72h
B
LPS+SIL
LPS+SIL+si-NC
LPS+SIL+si-Nrf2
Number of colonies
C
DAPI
EDU
Merge
EdU-positive cells(%)
D
apoptosis rate(%)
LPS+SIL+siNC
LPS+SIL+siNrf2
E
Bax
Bcl2
GAPDH
LPS+SIL-si-NC
LPS+SIL-si-Nrf2
Relative expression of Bax
Relative expression of Bcl-2
F
IL-1β(pg/mL)
IL-6(pg/mL)
TNF-α(pg/mL)
IL-17(pg/mL)

Figure 7. SIL inhibited LPS-induced myocardial injury and inflammation by activating the Nrf2/SLC7A11/GPX4 signaling pathway. A. Cell activity measured by CCK-8 assay. B. Colony formation assay for cell proliferation. C. EdU staining for cell proliferation. D. Flow cytometry analysis of cell apoptosis. E. WB analysis of apoptosis-related proteins. F. ELISA for inflammatory cytokine levels. $^{**}P < 0.01$, $^{***}P < 0.001$, vs. LPS + SIL-si-NC.

pathway to cardioprotection. Wang et al. reported that prostaglandin E receptor 1 (EP1) protects cardiomyocytes by activating Nrf2-mediated transcription of GPX4 and SLC7A11 [36], while hydrogen sulfide (H_2S) donors have been shown to activate the SLC7A11/GSH/GPX4 antioxidant pathway, thereby alleviating cardiac injury in rat cardiomyocytes [37]. In this study, SIL treatment significantly upregulated the protein expression of Nrf2, SLC7A11, and GPX4 in RA rat myocardial tissue. Conversely, suppression of Nrf2 led to reduced levels of SLC7A11 and GPX4, as evidenced by RT-qPCR, WB, and IHC results. Furthermore, cell experiments showed that Nrf2 knockdown markedly diminished SIL-induced enhancement of cell viability and proliferation compared to SIL treatment alone. Collectively, these results confirm that SIL alleviates myocardial injury and inflammation in RA by activating the Nrf2/SLC7A11/GPX4 signaling pathway.

Conclusion

This study elucidated the molecular mechanism underlying the therapeutic effects of SIL in RA, demonstrating that SIL exerts cardioprotective and anti-inflammatory effects primarily through activation of the Nrf2/SLC7A11/GPX4 signaling pathway. These findings are of great significance for understanding the role of SIL in the treatment of RA and its cardiovascular complications. Nevertheless, further clinical studies are needed to confirm the efficacy and safety of SIL in the treatment of RA and RA-related cardiac injury.

Acknowledgements

This work was supported by Shanghai Baoshan Hospital of Integrated Traditional Chinese and Western Medicine (BSZK-2023-Z02).

Disclosure of conflict of interest

None.

Address correspondence to: Dr. Xuzhou Duan, Department of Orthopedics, The First Affiliated Hospital of Naval Medical University, 168 Changhai Road, Yangpu District, Shanghai 200433, China. E-mail: duanxuzhou153@163.com

References

[1] Di Matteo A, Bathon JM and Emery P. Rheumatoid arthritis. Lancet 2023; 402: 2019-2033.

[2] Brown P, Pratt AG and Hyrich KL. Therapeutic advances in rheumatoid arthritis. BMJ 2024; 384: e070856.

[3] Jayatilleke A. Arthritis: rheumatoid arthritis. FP Essent 2025; 548: 25-30.

[4] Weber B, He Z, Yang N, Playford MP, Weisenfeld D, Iannaccone C, Coblyn J, Weinblatt M, Shadick N, Di Carli M, Mehta NN, Plutzky J and Liao KP. Divergence of cardiovascular biomarkers of lipids and subclinical myocardial injury among rheumatoid arthritis patients with increased inflammation. Arthritis Rheumatol 2021; 73: 970-979.

[5] Nie Q, Luo Q, Yan W, Zhang T, Wang H and Wu J. Rheumatoid arthritis and coronary atherosclerosis: a two-sample Mendelian randomization study. Front Cardiovasc Med 2023; 10: 1033644.

[6] Karpouzas GA, Estis J, Rezaeian P, Todd J and Budoff MJ. High-sensitivity cardiac troponin I is a biomarker for occult coronary plaque burden and cardiovascular events in patients with rheumatoid arthritis. Rheumatology (Oxford) 2018; 57: 1080-1088.

[7] Mahmoudi M, Aslani S, Fadaei R and Jamshidi AR. New insights to the mechanisms underlying atherosclerosis in rheumatoid arthritis. Int J Rheum Dis 2017; 20: 287-297.

[8] Popescu D, Rezus E, Badescu MC, Dima N, Seritean Isac PN, Dragoi IT and Rezus C. Cardiovascular risk assessment in rheumatoid arthritis: accelerated atherosclerosis, new biomarkers, and the effects of biological therapy. Life (Basel) 2023; 13: 319.

[9] Wadhwa K, Pahwa R, Kumar M, Kumar S, Sharma PC, Singh G, Verma R, Mittal V, Singh I, Kaushik D and Jeandet P. Mechanistic insights into the pharmacological significance of silymarin. Molecules 2022; 27: 5327.

[10] Zhao Y, Zhou Y, Gong T, Liu Z, Yang W, Xiong Y, Xiao D, Cifuentes A, Ibanez E and Lu W. The clinical anti-inflammatory effects and underlying mechanisms of silymarin. iScience 2024; 27: 111109.

[11] Surai PF, Surai A and Earle-Payne K. Silymarin and inflammation: food for thoughts. Antioxidants (Basel) 2024; 13: 98.

[12] Ghahfarrokhi SH, Heidari-Soureshjani S, Sherwin CMT and Azadegan-Dehkordi Z. Efficacy and mechanisms of silybum marianum, silymarin, and silibinin on rheumatoid arthritis

and osteoarthritis symptoms: a systematic review. Curr Rheumatol Rev 2024; 20: 414-425.
[13] Gabrielová E, Křen V, Jabůrek M and Modriansk ý M. Silymarin component 2,3-dehydrosilybin attenuates cardiomyocyte damage following hypoxia/reoxygenation by limiting oxidative stress. Physiol Res 2015; 64: 79-91.
[14] Rao PR and Viswanath RK. Cardioprotective activity of silymarin in ischemia-reperfusion-induced myocardial infarction in albino rats. Exp Clin Cardiol 2007; 12: 179-187.
[15] Zhao WK, Zhou Y, Xu TT and Wu Q. Ferroptosis: opportunities and challenges in myocardial ischemia-reperfusion injury. Oxid Med Cell Longev 2021; 2021: 9929687.
[16] Xu S, Wu B, Zhong B, Lin L, Ding Y, Jin X, Huang Z, Lin M, Wu H and Xu D. Naringenin alleviates myocardial ischemia/reperfusion injury by regulating the nuclear factor-erythroid factor 2-related factor 2 (Nrf2)/system xc-/glutathione peroxidase 4 (GPX4) axis to inhibit ferroptosis. Bioengineered 2021; 12: 10924-10934.
[17] Ding S, Duanmu X, Xu L, Zhu L and Wu Z. Ozone pretreatment alleviates ischemiareperfusion injury-induced myocardial ferroptosis by activating the Nrf2/Slc7a11/Gpx4 axis. Biomed Pharmacother 2023; 165: 115185.
[18] Jia C, Zhang Z, Wang J and Nie Z. Silymarin protects the rats against paraquat-induced acute kidney injury via Nrf2. Hum Exp Toxicol 2022; 41: 9603271221074334.
[19] Guo J, Wang S, Wan X, Liu X, Wang Z, Liang C, Zhang Z, Wang Y, Yan M, Wu P, Fang S and Yu B. Mitochondria-derived methylmalonic acid aggravates ischemia-reperfusion injury by activating reactive oxygen species-dependent ferroptosis. Cell Commun Signal 2024; 22: 53.
[20] Zhao H, Gu Y and Chen H. Propofol ameliorates endotoxin-induced myocardial cell injury by inhibiting inflammation and apoptosis via the PPARγ/HMGB1/NLRP3 axis. Mol Med Rep 2021; 23: 176.
[21] Kobayashi M, Ferreira MB, Costa RQ, Fonseca T, Oliveira JC, Marinho A, Carvalho HC, Girerd N, Rossignol P, Zannad F, Rodrigues P and Ferreira JP. Circulating biomarkers and cardiac structure and function in rheumatoid arthritis. Front Cardiovasc Med 2021; 8: 754784.
[22] Zambrano Zambrano A, Del Rio Zanatta H, Gonzalez Espinoza A, Bernal Alferes B, Zambrano Zambrano K, Martinez Salazar J and Ixcamparij Rosales CH. Heart failure in rheumatoid arthritis: clinical implications. Curr Heart Fail Rep 2024; 21: 530-540.
[23] Soleimani V, Delghandi PS, Moallem SA and Karimi G. Safety and toxicity of silymarin, the major constituent of milk thistle extract: an updated review. Phytother Res 2019; 33: 1627-1638.
[24] Moudgil KD and Venkatesha SH. The anti-inflammatory and immunomodulatory activities of natural products to control autoimmune inflammation. Int J Mol Sci 2022; 24: 95.
[25] Tong WW, Zhang C, Hong T, Liu DH, Wang C, Li J, He XK and Xu WD. Silibinin alleviates inflammation and induces apoptosis in human rheumatoid arthritis fibroblast-like synoviocytes and has a therapeutic effect on arthritis in rats. Sci Rep 2018; 8: 3241.
[26] Meng S, Yang F, Wang Y, Qin Y, Xian H, Che H and Wang L. Silymarin ameliorates diabetic cardiomyopathy via inhibiting TGF-β1/Smad signaling. Cell Biol Int 2019; 43: 65-72.
[27] Safarpour S, Safarpour S, Moghadamnia AA, Kazemi S, Ebrahimpour A, Shirafkan F, Mansoori R and Golchoobian R. Cardioprotective effect of silymarin nanoemulsion on 5-fluorouracil-induced cardiotoxicity in rats. Arch Pharm (Weinheim) 2022; 355: e2200060.
[28] Bayat G, Mazloom R, Hashemi SA, Pourkhalili K, Fallah P, Shams A, Esmaeili P and Khalili A. Silymarin administration attenuates cirrhotic-induced cardiac abnormality in the rats: a possible role of β(1)-adrenergic receptors and L-type voltage-dependent calcium channels. Iran J Med Sci 2022; 47: 367-378.
[29] Li W, Qu X, Kang X, Zhang H, Zhang X, Hu H, Yao L, Zhang L, Zheng J, Zheng Y, Zhang J and Xu Y. Silibinin eliminates mitochondrial ROS and restores autophagy through IL6ST/JAK2/STAT3 signaling pathway to protect cardiomyocytes from doxorubicin-induced injury. Eur J Pharmacol 2022; 929: 175153.
[30] Okiljevic B, Zdravkovic R, Preveden A, Preveden M, Mladenovic N and Susak S. The effect of silymarin on the prevention of atrial fibrillation after coronary artery bypass grafting. Braz J Cardiovasc Surg 2024; e20230422: e20230422.
[31] Dodson M, Castro-Portuguez R and Zhang DD. NRF2 plays a critical role in mitigating lipid peroxidation and ferroptosis. Redox Biol 2019; 23: 101107.
[32] Yan Y, Teng H, Hang Q, Kondiparthi L, Lei G, Horbath A, Liu X, Mao C, Wu S, Zhuang L, James You M, Poyurovsky MV, Ma L, Olszewski K and Gan B. SLC7A11 expression level dictates differential responses to oxidative stress in cancer cells. Nat Commun 2023; 14: 3673.
[33] Bersuker K, Hendricks JM, Li Z, Magtanong L, Ford B, Tang PH, Roberts MA, Tong B, Maimone TJ, Zoncu R, Bassik MC, Nomura DK, Dixon SJ and Olzmann JA. The CoQ oxidoreductase FSP1 acts parallel to GPX4 to inhibit ferroptosis. Nature 2019; 575: 688-692.
[34] Li N, Jiang W, Wang W, Xiong R, Wu X and Geng Q. Ferroptosis and its emerging roles in cardio-

vascular diseases. Pharmacol Res 2021; 166: 105466.
[35] Miao Y, Chen Y, Xue F, Liu K, Zhu B, Gao J, Yin J, Zhang C and Li G. Contribution of ferroptosis and GPX4's dual functions to osteoarthritis progression. EBioMedicine 2022; 76: 103847.
[36] Wang B, Jin Y, Liu J, Liu Q, Shen Y, Zuo S and Yu Y. EP1 activation inhibits doxorubicin-cardiomyocyte ferroptosis via Nrf2. Redox Biol 2023; 65: 102825.
[37] Zhang H, Pan J, Huang S, Chen X, Chang ACY, Wang C, Zhang J and Zhang H. Hydrogen sulfide protects cardiomyocytes from doxorubicin-induced ferroptosis through the SLC7A11/GSH/GPx4 pathway by Keap1 S-sulfhydration and Nrf2 activation. Redox Biol 2024; 70: 103066.